AIP | Journal of Applied Physics

Structural properties and spatial ordering in multilayered ZnMgTe/ZnSe type-II quantum dot structures

U. Manna, I. C. Noyan, Q. Zhang, I. F. Salakhutdinov, K. A. Dunn et al.

Citation: J. Appl. Phys. **111**, 033516 (2012); doi: 10.1063/1.3681812
View online: http://dx.doi.org/10.1063/1.3681812
View Table of Contents: http://jap.aip.org/resource/1/JAPIAU/v111/i3
Published by the American Institute of Physics.

Structural properties and spatial ordering in multilayered ZnMgTe/ZnSe type-II quantum dot structures

U. Manna,[1,a)] I. C. Noyan,[1] Q. Zhang,[2] I. F. Salakhutdinov,[1,4] K. A. Dunn,[3] S. W. Novak,[3] R. Moug,[2] M. C. Tamargo,[2,5] G. F. Neumark,[1] and I. L. Kuskovsky[4,5,b)]
[1]*Department of Applied Physics and Applied Mathematics, Columbia University, New York, New York 10027, USA*
[2]*Department of Chemistry, City College of CUNY, New York, New York 10031, USA*
[3]*College of Nanoscale Science and Engineering, University at Albany-SUNY, Albany, New York 12203, USA*
[4]*Department of Physics, Queens College of CUNY, Flushing, New York 11367, USA*
[5]*The Graduate Center of CUNY, New York, New York 10016, USA*

(Received 29 September 2011; accepted 7 January 2012; published online 8 February 2012)

We report the structural properties and spatial ordering of multilayer ZnMgTe quantum dots (QDs) embedded in ZnSe, where sub-monolayer quantities of Mg were introduced periodically during growth in order to reduce the valence band offset of ZnTe QDs. The periodicity, period dispersion, individual layer thickness, and the composition of the multilayer structures were determined by comparing the experimental high resolution x-ray diffraction (HRXRD) spectra to simulated ones for the allowed (004) and quasi-forbidden (002) reflections in combination with transmission electron microscopy (TEM) results. Secondary ion mass spectroscopy (SIMS) profiles confirmed the incorporation of Mg inside the QD layers, and the HRXRD analysis revealed that there is approximately 32% Mg in the ZnMgTe QDs. The presence of Mg contributes to higher scattering intensity of the HRXRD, leading to the observation of higher order superlattice peaks in both the (004) and (002) reflections. The distribution of scattered intensity in the reciprocal space map (RSM) shows that the diffuse scattered intensity is elongated along the q_x axis, indicating a vertical correlation of the dots, which is found to be less defined for the sample with larger periodicity. The diffuse scattered intensity is also found to be weakly correlated along the q_z direction indicating a weak lateral correlation of the dots. © *2012 American Institute of Physics*. [doi:10.1063/1.3681812]

I. INTRODUCTION

Obtaining adequate doping for good "bipolar" conductivity in wide-bandgap semiconductors, which is limited by poor solubility and/or excessive compensation, has been a problem over the decades.[1] Zn-Se-Te-based heterostructures are of interest for advancing the bipolar doping of difficult-to-dope ZnSe-based alloys,[2,3] since ZnSe can be readily doped n-type, while ZnTe can be doped p-type. Introduction of sub-monolayer quantities of Te in ZnSe during migration enhanced molecular beam epitaxy (ME-MBE) growth led to the formation of type-II ZnTe quantum dots (QDs) embedded in ZnSe,[4] where electrons are located in the ZnSe and holes are confined in ZnTe. Incorporation of nitrogen in these ZnTe QDs as a co-dopant resulted in higher net acceptor concentrations (6×10^{18} cm^{-3}) than those achieved in pure ZnSe.[3] However, due to a large hole confinement energy within the QDs, free carriers could not be readily obtained in such samples. To further explore the possibility to enhance p-type doping in this material system, we have attempted to modify the QD bandgap by incorporating sub-monolayer quantities of Mg along with Te to form ZnMgTe instead of pure ZnTe QDs. The choice of Mg was made due to the absence of cation core d-electrons in MgTe, which increases the bandgap and lowers the valence band maximum relative to that of ZnTe,[5,6] reducing the valence band offset with ZnSe.[6,7] This in turn is expected to reduce the hole confinement energy, and hence to enhance the p-type conductivity. A hole free-carrier concentration of the order of mid-10^{15} cm^{-3} has been measured,[8] for the first time, in such samples.

ZnTe/ZnSe multiple quantum dot (QD), quantum well (QW), and superlattice (SL) structures with type-II staggered band alignment have been previously grown with the aim of achieving tunable optical properties via quantum confinement effects.[4,9–11] The carrier confinement in type-II systems, such as ZnTe/ZnSe is independent of the bandgaps of the underlying materials, but rather depends on the band offsets. Thus, incorporation of Mg in this material system will allow us to control band offsets, hence the confinement energies, as well as to engineer the ZnTe/ZnSe bandgaps at the nanoscale. Modification of the valance band-offsets in this material system will also allow us to control the intermediate band lying within the forbidden energy gap of these materials to absorb photon energies below the semiconductor bandgap, and possibly increase the efficiency of intermediate bandgap solar cells.[12]

In this paper, we report the results of the structural analysis of multilayer ZnMgTe/ZnSe QD structures, and investigate the vertical and lateral ordering of the ZnMgTe QDs for two samples with different periodicities and different total number of periods: sample A consisting of 100 periods and sample B consisting of 200 periods. The transmission electron microscope (TEM) micrographs clearly show the presence of a modulated structure along the growth direction

a)Electronic mail: um2124@columbia.edu.
b)Electronic mail: Igor.Kuskovsky@qc.cuny.edu.

with the average thickness of each period being 3.66 and 4.82 nm for samples A and B, respectively. The secondary ion mass spectrometry (SIMS) profiles show small scale oscillations in Mg signal throughout the multiple QD structure layers in agreement with the incorporation of Mg inside the QD layer. SL peaks up to the fifth order are observed in high resolution x-ray diffraction (HRXRD) spectra arising from interference between each of the layers for primary (004) as well as quasi-forbidden (002) reflections. The periodicity, period dispersion, individual layer thickness, and the composition of the multi-layers were determined by comparing the experimental spectra to simulated ones for both the (004) and (002) reflections, assuming the QD array as an effective layer, whose scattering factor is an average of the scattering factors of the dots and the crystal matrix. The simulation results show that the average thickness of the layers containing ZnMgTe QDs is about 0.1 nm for both the samples, whereas the average thickness of the ZnSe spacers is about 3.6 and 4.1 nm for sample A and B, respectively. The analysis also revealed that there is approximately 32% Mg inside the ZnMgTe QDs, which contributes to the higher scattering intensity, and hence to the observation of higher order superlattice peaks in both the (004) and (002) reflections. Finally, the distribution of the scattered intensity in reciprocal space mapping (RSM) shows that the diffuse scattered intensity is elongated along the q_x axis indicating a vertical correlation of the dots, which is found to be less defined for sample B. The degree of vertical correlation decreases in sample B with increased periodicity (spacer thickness) even though the number of periods is doubled. The diffuse scattered intensity is also found to be weakly correlated along the q_z direction indicating a weak lateral correlation of the dots.

II. GROWTH DETAILS

The multilayer ZnMgTe/ZnSe structure shown schematically in Fig. 1(a) was grown on (001) GaAs substrates in a Riber 2300 molecular beam epitaxy (MBE) system. The ZnMgTe QDs were formed by exposing the growing surface to alternate elements, a technique commonly known as ME-MBE following procedures described elsewhere.[3,8] Here, we just point out the differences arising from addition of Mg to the QDs. After growing the ZnSe barrier (<10 MLs) by opening the Zn and Se shutters together for 35 s, ZnMgTe QDs were grown by employing three cycles of shutter operations as shown in Fig. 1(b). In cycle-1, following the ZnSe spacer growth, the Zn shutter was kept opened for 5 s followed by a 5 s growth interruption to desorb the excess Zn from the surface. After that, the Te shutter was opened to deposit submonolayer quantities of Te on the Zn-terminated surface for 5 s, followed by another 5 s growth interruption. Cycle-2 was almost identical to cycle-1, except that during the deposition of Zn, the Mg shutter was opened simultaneously, to deposit small quantities of Mg along with Zn. Cycle-3 was identical to cycle-1. This shutter operation produces sequential deposition of the elements, which, combined with the short interruptions, give rise to enhanced surface migration and the formation of self-assembled ZnMgTe QDs. These QDs are analogous to those observed by TEM, photoluminescence (PL), and magneto-PL measurements for ZnTe QDs.[2,4,8,13] The alternating ZnSe spacer layer and ZnMgTe QD depositions were repeated 100 times for sample A and 200 times for sample B in order to obtain multi-layers thick enough for characterization.

III. RESULTS AND DISCUSSION

A. TEM and SIMS results

Cross-sectional TEM specimens were prepared by a conventional *in situ* dual beam lift-out method using a 30 keV Ga^+ focused ion beam after a deposition of 1 μm thick Pt as a surface protection layer. TEM micrographs were recorded in high vacuum using a JEOL 2010 F microscope operated at 200 keV. Figure 2 shows the cross-sectional TEM images of samples A and B. The micrographs clearly show the presence of a modulated structure with a period of 3.66 ± 0.06 nm and 4.82 ± 0.02 nm for samples A and B, respectively, along the growth direction, while this modulation is absent in the buffer layer as well as in the ZnSe cap layer and substrate (not shown). The thickness of the periods decreases by about 7% for sample A, and by

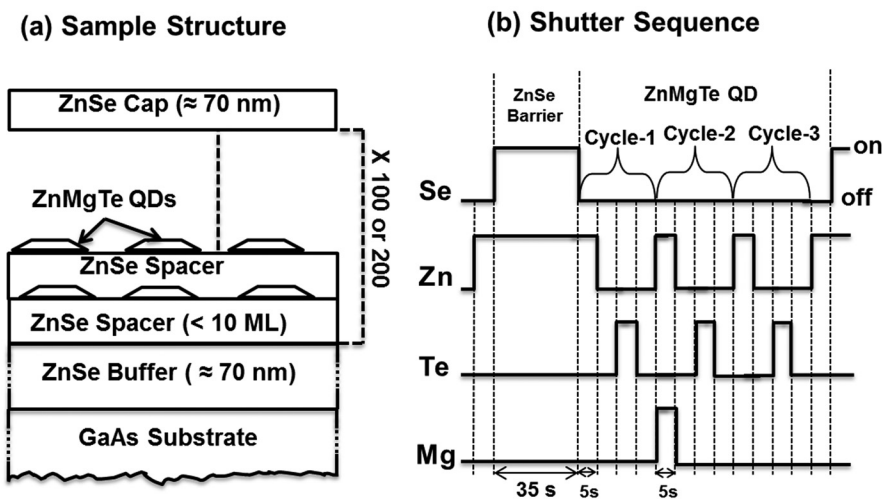

FIG. 1. (a) Schematic of the sample structure, and (b) shutter sequence employed during migration enhanced molecular beam epitaxy (ME-MBE) growth of the sample.

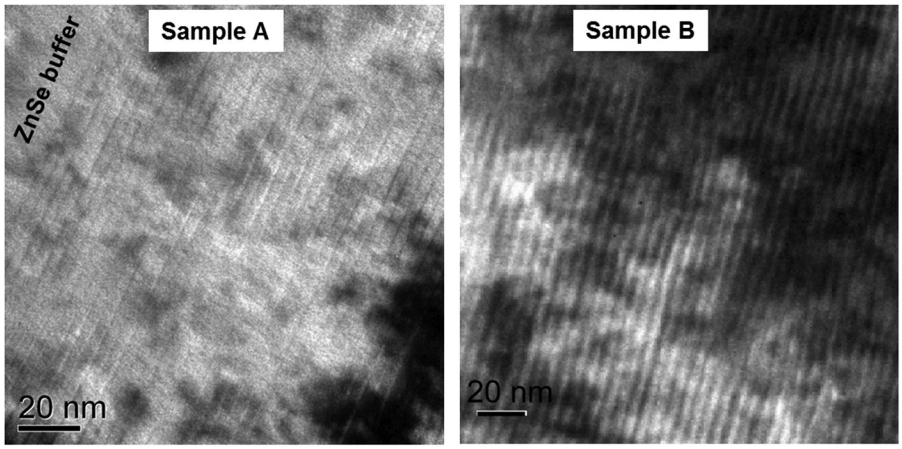

FIG. 2. TEM images showing modulated structure along the growth direction in the superlattice region for both the samples.

about 9% for sample B from the layers grown first, near the substrate interface to the final layers near the surface. The calculated thickness values obtained from the TEM were taken as a starting point for simulation of the HRXRD data as discussed in Sec. III B. We note that the TEM data does not directly show the presence of quantum dots because of low contrast between ZnSe and ZnMgTe and the small size of the dots.

SIMS analysis was carried out using an IonTOF-V time-of-flight system. The analysis beam was a pulsed Bi^+ (25 keV, incidence angle 45°) and the sputtering beam was Cs (2 keV, incidence angle 45°). Secondary ions were accepted from the central $50 \times 50\,\mu$m of the sputter crater with positive Cs cluster secondary ions detected. Figure 3 shows the depth-resolved Mg profiles recorded for the ZnMgTe/ZnSe samples A and B. The depth scale was calibrated by setting the thickness of the cap layer to 77 nm as determined by TEM. The small scale oscillations of the Mg signal within the multi-QD layer structure clearly indicate presence of Mg in the modulated structure, and also suggest that Mg is preferentially located inside the QD layer. For sample A, the oscillations are present throughout the sample, while for sample B the small scale oscillations are clear only near the surface. In sample B, there are large variations in the Mg signal below 200 nm, possibly due to problems with the growth shuttering sequence. The small scale oscillations occur with an average period thickness of 2.3 and 2.7 nm for samples A and B, respectively. These values are different from the thickness of the average periods as deduced from the TEM results because of sputtering rate differences between materials, which cause the SIMS depth scale to be different from the true layer thickness.[14]

B. HRXRD analysis

HRXRD is a non-destructive technique that can be used to determine layer-specific thickness, lattice parameter, strain, composition, and defect densities of superlattice and multilayered semiconductor structures.[15–17] HRXRD measurements were carried out at Beamline X20A at the National Synchrotron Light Source (NSLS) at the Brookhaven National Laboratory (BNL). All measurements were performed using monochromatic synchrotron radiation at 8 keV ($\lambda = 1.54056$ Å), with a double-crystal Ge (111) monochromator. The incident beam size was set to about 1×1 mm^2. The diffracted beam path consisted of scatter slits, followed by a Si (111) analyzer in front of the detector. ω-2θ scans for symmetric (004) and (002), and asymmetric (224) reflections were measured. The experimental ω-2θ curves were analyzed by the commercially available BEDE RADS program. For reciprocal space map measurements, a series of ω-2θ scans, each offset by $\delta\omega \sim 0.04°$ were performed.

The experimental and simulated ω-2θ curves for the ZnMgTe/ZnSe multilayer structure are shown in Figs. 4 and

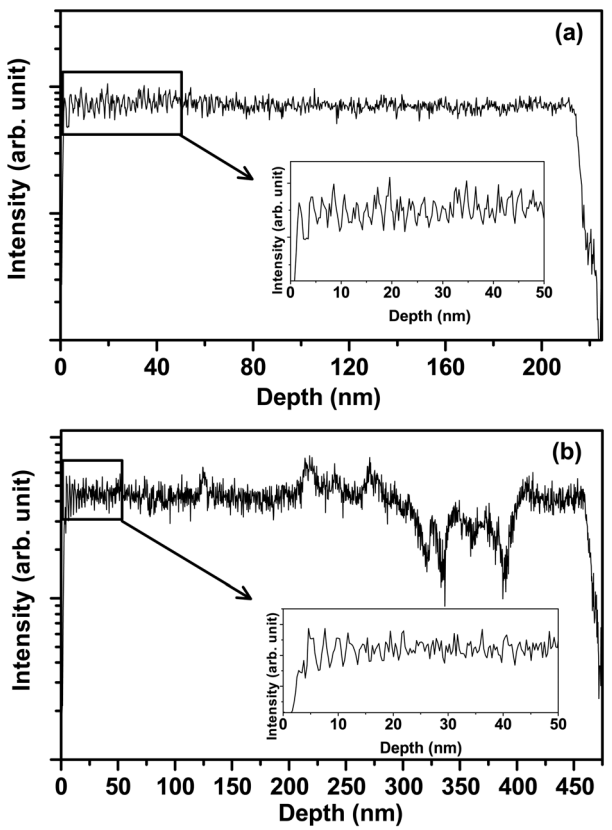

FIG. 3. SIMS profiles for the sample A consisting of 100 periods (a) and sample B consisting of 200 periods (b) showing periodic variations in Mg content.

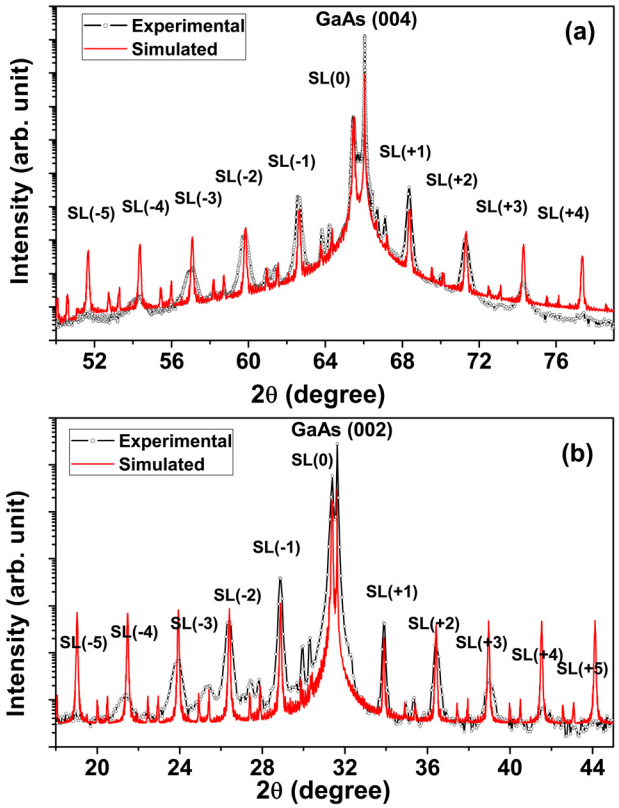

FIG. 4. (Color online) The experimental and simulated ω-2θ curves for the (004) (a) and (002) (b) reflections for sample A, which consists of 100 periods.

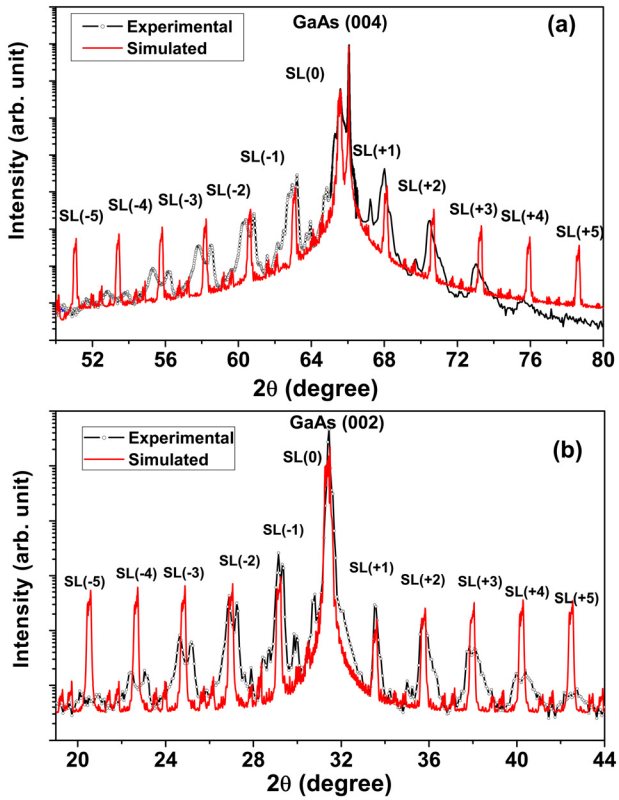

FIG. 5. (Color online) The experimental and simulated ω-2θ curves for the (004) (a) and (002) (b) reflections for sample B, which consists of 200 periods.

5 for samples A and B, respectively, for both the (004) and (002) reflections. The quasi-forbidden (002) reflection is observed in compound materials, such as GaAs or ZnSe, due to small differences in the electronic scattering factors of the constituent elements. The peaks marked as SL(0) at around 66.5° for the (004) reflection and 31.3° for the (002) reflection are caused by the Bragg reflections from the combined ZnSe spacers and ZnMgTe QDs of the multilayer system. The spacing between the SL(0) and the substrate peak is proportional to the relative difference of the vertical lattice constant of the substrate and the averaged lattice constant of the multilayer structure. A set of subsidiary satellite peaks arising from interference between each of the layers is observed, up to the fifth order, symmetrically around the SL(0) peak for both the (004) and (002) reflections for both of the samples. The small intermediate peaks between the SL satellite peaks are believed to arise from fluctuation of Te within the QDs along the growth direction.

To extract the structural parameters in our multilayer structure, the experimental ω-2θ curves were simulated by a commercially available BEDE RADS program based on Takagi[18] and Taupin[19] generalized dynamical diffraction theory after an estimation of the initial fitting parameters as follows. The average lattice parameter along the growth direction, $\langle c \rangle$ is calculated directly from the SL(0) peak of the ω-2θ curve using Bragg's law. We assumed that the stresses in the epitaxial layers are equal biaxial in the plane of the film, i.e., the unit cell is deformed from cubic to tetragonal. For a tetragonal unit cell, the average in-plane lattice parameter $\langle a \rangle$ can be calculated from $1/d^2_{224} = [(2^2 + 2^2)/a^2] + (4^2/c^2)$, where d_{224} is calculated from the SL(0) of the asymmetric (224) reflection (not shown here). From the values of $\langle a \rangle$, $\langle c \rangle$ and Poisson's ratio, we estimate the average composition of Mg within the structure assuming a linear dependence of lattice parameters on composition. The thickness of each period, the cap layer and the buffer layer were estimated from the TEM results as discussed above. The process of estimation of the initial fitting parameters has been described elsewhere in detail.[15,16,20]

Figures 4 and 5 show that there is an excellent agreement between the experimental and simulated curves for both the (004) and (002) reflections; the refined simulation parameters are listed in Table I. It should be noted that the (002) reflection was simulated with the same fitting parameters as (004) except for strains in the different layers. For simulation purposes, we replaced the QD array by an effective layer, whose scattering factor is an average of the scattering factors of the dots and the crystal matrix. The simulation results show that the average thickness of the effective QD layer is about 0.1 nm, and the average thicknesses of the spacers are about 3.6 and 4.1 nm for samples A and B, respectively. Hence, the average thicknesses of each period in samples A and B are about 3.7 and 4.2 nm, respectively, which is in good agreement with the TEM results. The experimental higher order SL peaks are broadened compared to the SL(0) peak, an effect which is more pronounced in sample B. This indicates a periodic dispersion in the sample along the growth direction, also observed in the TEM

TABLE I. The structural parameters for the ZnMgTe/ZnSe multilayer structures determined by the comparison of the experimental ω-2θ curves to the simulated ones for (004) and (002) reflections. The parameters t_A and t_B are the thickness of the different layers in samples A and B, respectively, and x and y are the compositions of Mg and Te in the QDs and spacers, respectively.

Layer	t_A (nm)	t_B (nm)	x (%)	y (%)
ZnSe (Cap)	77±5	87±3	···	···
$Zn_{1-x}Mg_xTe$ (QD)	0.1±0.01	0.1±0.01	32±3	···
$ZnTe_ySe_{1-y}$ (Spacer)	3.6±0.1	4.1±0.1	···	0.8±0.2

measurement as discussed above. Note that the variation in spacer thickness (~15%) between the two samples, which were not grown sequentially, is within the reproducibility of the MBE growth process.

The simulation result also suggests that Te is mainly confined within the QD layers; there is a small amount of Te diffusion (<1%) inside the spacer, which is consistent with our previous measurements for the Zn-Te-Se system.[20] During simulation, we neglected the Mg diffusion inside the ZnSe spacer since Mg has a four orders of magnitude smaller diffusion coefficient than Te, as reported for diffusion inside GaAs.[21] However, we found that there is approximately 32% Mg inside the ZnMgTe QDs. We also note that addition of Mg in the QD layers contributed to the higher scattering intensity of the superlattice peaks as shown by comparing the normalized experimental curves for a sample grown without Mg (blue solid circle) to the data from the sample with Mg (black open circle) in the QD layers (sample A) shown in Fig. 6. The higher scattering intensity with the addition of Mg can be explained by formation of a strained interfacial layer[22,23] at the spacer and QD layer interface due to the larger lattice constant of ZnMgTe. On one side of the interfacial layer, the average lattice spacing can be assumed to be that of the spacer, i.e., ZnSeTe, whereas on the other side of the interfacial layer the average lattice constant can be assumed to be that of the QD layer, i.e., ZnMgTe. The structure factor, and hence the scattering intensity, is stronger for this case compared to the system without Mg because of a larger lattice mismatch. Higher scattering intensity with addition of Mg also leads to the observation of up to fifth order SL peaks as shown in Figs. 4 and 5 compared to the

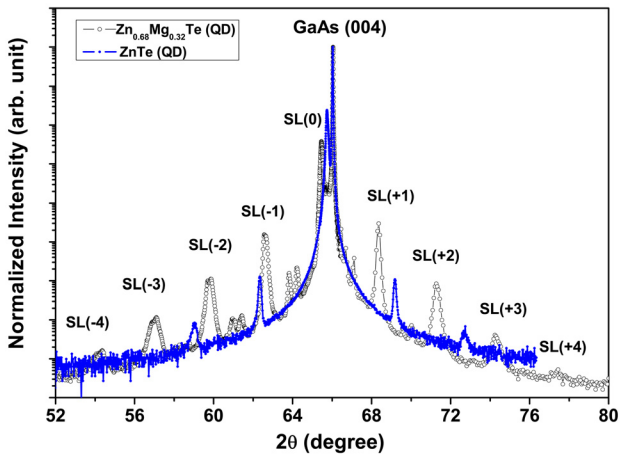

FIG. 6. (Color online) Experimental HRXRD curves for a sample grown with (sample A) and without Mg in the QD layer. Incorporation of Mg contributes to the higher scattering intensity, hence observation of higher order SL peaks.

Zn-Te-Se system, where SL peaks were visible only up to the second order as shown in Fig. 6. (see also Refs. 9 and 20).

C. Spatial ordering of the dots

HRXRD based RSMs have been previously used to observe vertical and lateral correlations, diffuse scattering due to strain fluctuations, and lateral peak broadening of the superlattice and multilayer structures containing quantum dots.[24–29] The RSM of the ZnMgTe/ZnSe multilayer hetero-structure consists of periodic superlattice peaks in the q_x direction arising from a finite correlation length of the multilayer structure, as shown in Figs. 7(a) and 7(b) for samples A and B, respectively, for the (002) reflection. The peak labeled S(002) corresponds to the diffraction from the substrate, and SL(n) is the nth superlattice peak of the multilayer structure with the spacing between the satellite peaks given by $2\pi/D$, where D is the superlattice period and n is an integer. The ZnMgTe QDs embedded in a ZnSe matrix give rise to diffuse scattering accompanying the coherent diffraction from the whole multilayer structure. The diffuse scattering is caused by the difference in the scattering factors of ZnMgTe and ZnSe and the elastic deformation strain field in the ZnSe matrix surrounding the dots. A theoretical description of the x-ray scattering from the QD

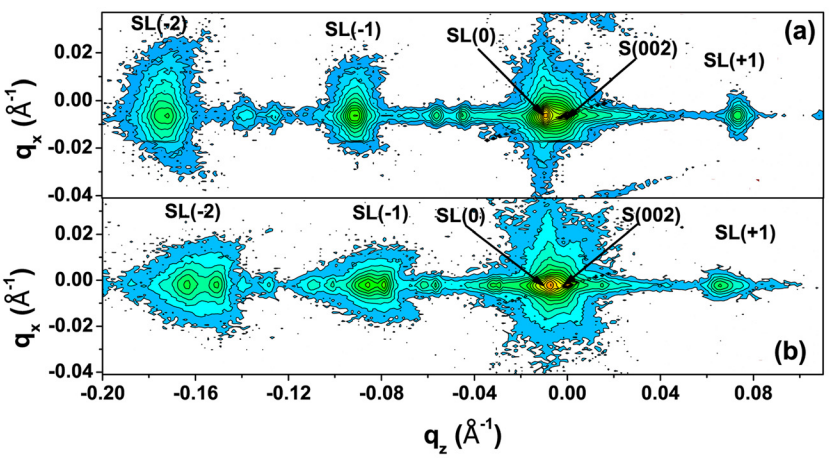

FIG. 7. (Color online) The reciprocal space map for the (002) reflection of the ZnMgTe/ZnSe multilayer structure for (a) sample A and (b) sample B.

arrays based on a statistical kinematical approach[25] showed that if the dots are fully correlated vertically, and if we neglect the surface stress relaxation, the q_z dependence of the scattered intensity is mainly determined by the structure factor of the multilayer structure. Thus, in RSM, the diffuse scattered intensity is correlated in "stripes" parallel to the q_x axis at the same positions $q_z = (2\pi n)/D$ as the coherent superlattice maxima. On the other hand, if the dots are completely uncorrelated vertically, the scattered intensity is rather broad, and exhibits no stripe-like structure.[25] The diffuse scattered intensity for the sample A consisting of 100 periods with 3.6 nm spacer is elongated along the q_x direction axis as shown in Fig. 7(a), which is found to be broadened along the q_z direction for sample B, which consists of 200 periods with a 4.1 nm spacer. This indicates that the ZnMgTe QDs for the sample A are strongly correlated vertically compared to sample B even though the number of periods is doubled for the latter case.

The lattice deformations of the ZnSe matrix around the buried ZnMgTe QDs produce a non-uniform strain distribution on the epitaxial surface of each layer containing QDs due to the difference in the lattice constant between the ZnMgTe QDs and ZnSe spacer. The interlayer correlation, that is, the ordering mechanism is dominated by the long-range elastic interactions between the strained ZnMgTe QDs providing a driving force for spatially correlated dot nucleation. The preferred dot nucleation takes place at the local minima of the non-uniform strain distribution energy that is spatially correlated to the dot positions in the previous layer. As a result, long-range vertical correlations of the QDs across the spacers are formed.[30,31] The superposition of the strain fields of neighboring QDs may also result in a lateral ordering of the dots.[32] For smaller spacer thicknesses, the strain energy above the buried dot has deeper energy minima, as a result, more deposited adatoms are attracted to the minima position, hence there is a larger probability of dot correlation along the growth direction.[30,31] With increasing spacer thickness, the depth of the energy minima decreases, as a result, the paring probability decreases. This leads to a reduced vertical correlation for the sample B having larger spacer thickness. On the other hand, with increasing number of periods, the QD size increases and becomes progressively more uniform, which should gradually increase the vertical correlation of the dots.[32–34] However, in the far-field limit, when the spacer thickness exceeds about two times the height of the dots as in our case, the actual size and shape of the dots can be ignored, that is, the dots can be treated as simple point stress sources.[35] Hence, a deeper strain energy minimum due to decreased spacer thickness is mainly responsible for the increased vertical correlation in sample A. However, it cannot be ruled out that other factors may be affecting the reduced vertical correlation observed in sample B. A systematic study will be required in order to fully quantify the dependency of vertical correlation of QDs on spacer thickness.

The lateral arrangement of the dots also give rise to lateral intensity satellites at the positions $q_x = (2\pi p)/L$, where L is the mean dot distance, and p is an integer.[25,36] For the investigated ZnMgTe/ZnSe multilayer structure, we did not find any lateral intensity satellites, possibly because of the low density of the dots in our samples. However, the diffuse scattered intensity along the q_z direction is found to be weakly correlated as shown in Fig. 7(a) for sample A indicating a weak lateral correlation of the dots. For sample B, the diffuse scattered intensity along the q_z direction is found to be correlated further as shown in Fig. 7(b). With increasing dot size and uniformity, the increase in superposition of the strain fields of neighboring dots results in a relatively stronger lateral ordering of the dots. However, a spectrally broad luminescence has been observed due to the fluctuations in dots size and composition, hence distribution of the density of states over a wide energy range, as well as due to strong electron-phonon coupling.[8,37]

IV. CONCLUSIONS

In summary, we have determined the periodicity, period dispersion, individual layer thickness, and the composition of the ZnMgTe/ZnSe multilayer structures by comparing the experimental HRXRD spectra to simulated ones in combination with TEM. The presence of Mg preferentially inside the ZnMgTe QDs was confirmed by SIMS measurements, while the HRXRD analysis revealed that there is approximately 32% Mg inside the ZnMgTe QDs. The presence of Mg contributes to higher scattering intensity, leading to the observation of higher order superlattice peaks in both the (004) and (002) reflections. The distribution of the diffuse scattered intensity in both the q_x and q_z direction in the reciprocal space map indicates a correlation of the ZnMgTe dots embedded in ZnSe in both the vertical and lateral directions with the degree of vertical correlation strongly dependent on the spacer thickness. This study will enable us to better control the MBE growth parameters in order to manipulate the bandgaps, band offsets, and degree of correlations of ZnTe/ZnSe type-II QDs by incorporation of Mg within the QDs. These materials have possible applications to doping of other difficult-to-dope systems, the design of intermediate band solar cells, and the manipulation of type-II magneto-excitons.

ACKNOWLEDGMENTS

This research was supported by the U.S. Department of Energy, Office of Basic Energy Sciences, Division of Materials Sciences and Engineering under Award No. DE-FG02-10ER46678. Use of the National Synchrotron Light Source at Brookhaven National Laboratory (BNL) was supported by the U.S. Department of Energy, Office of Science, Office of Basic Energy Sciences, under Contract No. DE-AC02-98CH10886. One of us (R.M.) acknowledges the support of the National Science Foundation under Award No. HRD-0833180 (CREST-CENSES).The authors would like to thank Dr. Jean Jordan-Sweet, the manager of X20A beamline, and L. Li, M. Treger, S. M. Polvino, and A. J. Ying for useful discussions and assistance during the experiments at BNL.

[1]G. F. Neumark and R. M. Park, Phys. Today **47**, 26 (1994).
[2]I. L. Kuskovsky, Y. Gu, Y. Gong, H. F. Yan, J. Lau, I. C. Noyan, G. F. Neumark, O. Maksimov, X. Zhou, M. C. Tamargo, V. Volkov, Y. Zhu, and L. Wang, Phys. Rev. B **73**, 195306 (2006).
[3]W. Lin, S. P. Guo, M. C. Tamargo, I. Kuskovsky, C. Tian, and G. F. Neumark, Appl. Phys. Lett. **76**, 2205 (2000).
[4]Y. Gu, I. L. Kuskovsky, M. van der Voort, G. F. Neumark, X. Zhou, and M. C. Tamargo, Phys. Rev. B **71**, 045340 (2005).

[5]D. J. Chadi, Phys. Rev. Lett. **72**, 534 (1994).
[6]D. Segev and S.-H. Wei, Phys. Rev. B **68**, 165336 (2003).
[7]S.-H. Wei and A. Zunger, Appl. Phys. Lett. **72**, 2011 (1998).
[8]Q. Zhang, A. Shen, I. L. Kuskovsky, and M. C. Tamargo, J. Appl. Phys. **110**, 034302 (2011).
[9]Y. Gong, W. MacDonald, G. F. Neumark, M. C. Tamargo, and I. L. Kuskovsky, Phys. Rev. B **77**, 155314 (2008).
[10]M. C. Kuo, C. S. Yang, P. Y. Tseng, J. Lee, J. L. Shen, W. C. Chou, Y. T. Shih, C. T. Ku, M. C. Lee, and W. K. Chen, J. Cryst. Growth **242**, 533 (2002).
[11]K. Suzuki, U. Neukirch, J. Gutowski, N. Takojima, T. Sawada, and K. Imai, J. Cryst. Growth **184–185**, 882 (1998).
[12]A. Luque and A. Marti, Phys. Rev. Lett. **78**, 5014 (1997).
[13]I. L. Kuskovsky, W. MacDonald, A. O. Govorov, L. Mourokh, X. Wei, M. C. Tamargo, M. Tadic, and F. M. Peeters, Phys. Rev. B **76**, 035342 (2007).
[14]R. G. Wilson, F. A. Stevie, and C. W. Magee, in *Secondary Ion Mass Spectrometry: A Practical Handbook for Depth Profiling and Bulk Impurity Analysis* (Wiley, New York, 1989).
[15]D. K. Bowen and B. K. Tanner, in *High Resolution X-ray Diffractometry and Topography* (Taylor & Francis, London, 1998).
[16]P. F. Fewster, Semicond. Sci. Technol. **8**, 1915 (1993).
[17]M. A. Moram and M. E. Vickers, Rep. Prog. Phys. **72**, 036502 (2009).
[18]S. Takagi, Acta Crystallogr. **15**, 1311 (1962).
[19]D. Taupin, Bull. Soc. Fr. Mineral. Crystallogr. **87**, 469 (1964).
[20]Y. Gong, F. Y. Hanfei, I. L. Kuskovsky, Y. Gu, I. C. Noyan, G. F. Neumark, and M. C. Tamargo, J. Appl. Phys. **99**, 064913 (2006).
[21]B. L. Sharma, in *Handbook of Chemistry and Physics*, edited by W. M. Haynes (CRC Press, Boca Raton, 2011).
[22]E. E. Fullerton, I. K. Schuller, H. Vanderstraeten, and Y. Bruynseraede, Phys. Rev. B **45**, 9292 (1992).
[23]J. M. Vandenberg, M. B. Panish, H. Temkin, and R. A. Hamm, Appl. Phys. Lett. **53**, 1920 (1988).
[24]J. Stangl, V. Holy, and G. Bauer, Rev. Mod. Phys. **76**, 725 (2004).
[25]A. A. Darhuber, P. Schittenhelm, V. Holy, J. Stangl, G. Bauer, and G. Abstreiter, Phys. Rev. B **55**, 15652 (1997).
[26]N. Faleev, K. Pavlov, M. Tabuchi, and Y. Takeda, Jpn. J. Appl. Phys. **38**, 818 (1999).
[27]V. Holý, G. Springholz, M. Pinczolits, and G. Bauer, Phys. Rev. Lett. **83**, 356 (1999).
[28]V. Holy, A. A. Darhuber, J. Stangl, S. Zerlauth, F. Schaffler, G. Bauer, N. Darowski, D. Lubbert, U. Pietsch, and I. Vavra, Phys. Rev. B **58**, 7934 (1998).
[29]Th. Schmidt, E. Roventa, T. Clausen, J. I. Flege, G. Alexe, S. Bernstorff, C. Kübel, A. Rosenauer, D. Hommel, and J. Falta, Phys. Rev. B **72**, 195334 (2005).
[30]Q. Xie, A. Madhukar, P. Chen, and N. P. Kobayashi, Phys. Rev. Lett. **75**, 2542 (1995).
[31]G. Springholz, M. Pinczolits, V. Holy, S. Zerlauth, I. Vavra, and G. Bauer, Physica E **9**, 149 (2001).
[32]J. Tersoff, C. Teichert, and M. G. Lagally, Phys. Rev. Lett. **76**, 1675 (1996).
[33]T. Schmidt, T. Clausen, J. Falta, G. Alexe, T. Passow, D. Hommel, and S. Bernstorff, Appl. Phys. Lett. **84**, 4367 (2004).
[34]C. Teichert, M. G. Lagally, L. J. Peticolas, J. C. Bean, and J. Tersoff, Phys. Rev. B **53**, 16334 (1996).
[35]S. Mackowski, G. Karczewski, T. Wojtowicz, J. Kossut, S. Kret, A. Szczepanska, P. Dluzewski, G. Prechtl, and W. Heiss, Appl. Phys. Lett. **78**, 3884 (2001).
[36]V. Holy, A. A. Darhuber, G. Bauer, P. D. Wang, Y. P. Song, C. M. S. Torres, and M. C. Holland, Phys. Rev. B **52**, 8348 (1995).
[37]U. Manna, Q. Zhang, S. Dhomkar, I. F. Salakhutdinov, M. C. Tamargo, I. C. Noyan, G. F. Neumark, and I. L. Kuskovsky, "Radiative transitions in stacked ZnMgTe quantum dots embedded in ZnSe," (to be published).